AUTHOR(S): DROUBI, M.G., REUBEN, R.L. and STEEL, J.I.

TITLE: Flow noise identification using acoustic emission (AE) energy decomposition for sand monitoring in flow pipeline.

YEAR: 2018

Publisher citation: DROUBI, M.G., REUBEN, R.L. and STEEL, J.I. 2018. Flow noise identification using acoustic emission (AE) energy decomposition for sand monitoring in flow pipeline. Applied acoustics [online], 131, pages 5-15. Available from: https://doi.org/10.1016/j.apacoust.2017.10.016

OpenAIR citation: DROUBI, M.G., REUBEN, R.L. and STEEL, J.I. 2018. Flow noise identification using acoustic emission (AE) energy decomposition for sand monitoring in flow pipeline. Applied acoustics, 131, pages 5-15. Held on OpenAIR [online]. Available from: https://openair.rgu.ac.uk

Flow noise identification using acoustic emission (AE) energy decomposition for sand monitoring in flow pipeline

M. G. Droubi*[1], R. L. Reuben[2] and J. I. Steel[1]

[1] School of Engineering, Robert Gordon University, Aberdeen, AB10 7GJ, UK

[2] School of Engineering and Physical Sciences, Heriot-Watt University, Edinburgh, EH14 4AS, UK

*Corresponding author: Tel: +44 1224 262336, e-mail: m.g.droubi@rgu.ac.uk

Abstract

In pipelines used for petroleum production and transportation, sand particles may be present in the multi-phase flow of oil and gas and water. The Acoustic Emission (AE) measurement technique is used in the field of sand monitoring and detection in the oil and gas industry. However, as the AE signals recorded are strongly influenced by flow conditions in the pipe, identification of sand particle related signals or events remain a significant challenge in interpretation of AE signals. Therefore, a systematic investigation of sand particle impact AE energy measurements, using a sensor mounted on the outer surface of a sharp bend in a carbon steel pipe, was carried out in the laboratory to characterise flow signals using a slurry impingement flow loop test rig. A range of silica sand particles fractions of mean particle size (212 to 710 μm) were used in the flow with particle nominal concentration between (1 and 5 wt.%) while the free stream velocity was changed between (4.2 and 14 ms^{-1}).

A signal processing technique was developed in which the total AE energy associated with particle-free water impingement was divided into static and oscillated parts and a demodulated frequency analysis was carried out on the oscillated part to identify major spectral components and hence the sources of AE signals. A simple theoretical model for water impingement AE signals was then developed to show the dependence of AE energy components on different flow speeds. A similar decomposition of AE energy into static and oscillatory components was used to analyse AE signals for particle-laden flows. The effect of flow speed on the spectral AE energy for different sand concentrations and particle size fractions was investigated and the results show that the 100Hz band is attributed to mechanical noise, the 42Hz band is due to fluid turbulence and the dominant band is broad oscillated component.

The AE energy decomposition method together with the water impingement model and coupled with spectral peaks filtering enable isolation of AE energy associated with particle impact from other AE sources and noise and ,hence, the proposed decomposition approach can enhance the interpretation of AE data in pipeline flows.

Keywords: Acoustic Emission (AE), sand monitoring, slurry, flow noise.

List of symbols and abbreviations:

AE: acoustic emission

C: solids concentration in flow loop (expressed as weight percentage)

d_p: Diameter of impacting particle

RMS AE: Root-mean-square of the acoustic emission time series, often used as a time-series itself, of lower effective sampling rate)

wt.%: percentage, by weight (for example mass of particles as a percentage of total mass of particles plus carrier fluid)

v: fluid speed in flow loop

E^w: Measured AE energy associated with particle-free water impingement, V^2.sec

E_{st}^{w}: Static AE energy associated with particle-free water impingement, V^2.sec

E_{osc}^{w}: Oscillated AE energy associated with particle-free water impingement, V^2.sec

E_{tot}^{sl}: Measured AE energy associated with particle-laden flow, V^2.sec

E_{st}^{sl}: Static AE energy associated with particle-laden flow, V^2.sec

E_{osc}^{sl}: Oscillated AE energy associated with particle-laden flow, V^2.sec

E_{sp1}^{sl}: Oscillated AE energy associated with particle-laden flow for 100 Hz harmonic series, V^2.sec

E_{sp2}^{sl}: Oscillated AE energy associated with particle-laden flow for 42 Hz band, V^2.sec

E_{broad}^{sl}: Remaining oscillated AE energy associated with particle-laden flow, V^2.sec

E^P: AE energy associated with particle impacts, V^2.sec

E_{st}^{p}: Static AE energy associated with particle impacts, V^2.sec

n: curve fit power index, as in $y = Ax^n + B$

n_i: curve fit power index for a particular independent variable

1. Introduction

During petroleum production, sand particles may be present in hydrocarbon flow due to drilling, formation damage, well ageing, reservoir fracturing and use of proppants [1]. The sand can cause serious problems in wear of pipelines and valves and the integrity of the production facilities [2]. Therefore, methods of identifying and quantifying sand production are needed. Methods of sand management include inspection techniques after production and involving disrupting production. Faster, non-disruptive, on-line monitoring techniques for sand production are needed to enable hydrocarbon production optimization. An on-line technique needs to identify the onset of sand production, assess the extent of damage to pipelines and production facilities, enable actions to be taken when excessive sand is produced and provide timely information for sand management measures.

Existing sand monitoring techniques can be broadly classified as intrusive and non-intrusive methods. Electrical Resistance (ER) sensing elements, radio-active probes and optical measurements [3] use intrusive mechanism to monitor the presence of sand flow streams. This type of device can be inefficient as they are not robust and need replaced after establishing the sand presence. Although such methods provide a reasonable assessment of the cumulative sand production, they are not effective in providing the real time or instantaneous indication of sand production [4]. Therefore, there is a need for a non-intrusive, fast, easily and cheaply maintained technique that can monitor large structures or pipelines from a single sensor location. Non-intrusive methods involve "listening" to the sound generated by a stream of solid particles impinging on a pipe wall. Vibration analysis is a non-intrusive technique which has gained interest in recent years. For example, Wang et al [5] have used a vibration technique for sand detection in sand-oil-water multiphase flow. A multiphase flow comprising a mixed liquid of 80 wt.% water and 20 wt.% oil with average speed of 2.14 ms^{-1} and sand content from 0.03 wt.% to 0.09 wt.% with sand fractions between 80 and 325 μm was used in a multiphase flow loop. A broad band vibration sensor was installed at two locations, a down-stream bend pipe wall and on an impact cell which was designed to amplify the vibration signals caused by solid particle impacts. They observed a good correlation between power spectrum amplitude of recorded vibration signals and sand concentration with different sizes of particles. In another work by the same authors, Wang et al [6] have used the vibration measurement technique for sand detection in sand-gas multiphase flow. Using the same vibration sensor to acquire the vibration signals generated by sand impinging on horizontal and vertical down-stream bend pipe wall, they observed a correlation between vibration energy and sand mass flow rate. Also,

Wang et al [7] carried out a more applied field study on four typical wells in Bohai oil production platform. They observed a difference in the time-frequency domain and power spectrum between sand and non-sand producing wells and claimed a correlation between the recorded vibration signal power spectrum amplitude and sand production volume.

Another non-intrusive technique is monitoring of particle impact using Acoustic Emission (AE) which exploits the fact that, when a hard, solid particle strikes a target, a fraction of the incident energy dissipates as elastic waves, which will propagate through the target material according to its geometry and elastic properties before being detected by a suitable AE sensor. Because of this, and the very high temporal resolution available from AE, the potential of AE to monitor particle impact energy has attracted many investigators. A detailed review on the application of AE in monitoring particle impacts and in wear studies is beyond the scope of this paper and has been presented in the author's previous works [8-11].

The characteristics of the observed signal from the AE sensor will depend not only on the particle impact dynamics, the propagation of waves into the target medium and the type of sensor used but also on the carrier fluid conditions as well as electrical noise that is produced by analog-to-digital conversion circuit. Therefore, to enhance the detection ability of sand particle impacts an understanding of other sources of AE associated with fluid flow [12] is needed, to enable detailed analysis of the signals. Generally speaking, there are two main methods to filter out the noise from various sources such as mechanical and flow related AE sources. The first is to use a band-pass filter in the hardware circuit where the piezoelectric element is tuned to magnify the response from a specific frequency range while attenuating the frequencies associated with other AE sources. However, this method can introduce an electrical noise from analog devices. The second method is to use signal processing algorithms after converting the analog signal to digital signal. This method was implemented in this work. Gao et al [4] mounted an acoustic sensor on the external surface of a bend in a 1 inch diameter pipe in a multiphase flow loop and varied flow speed between 5 to 9.5 ms^{-1} and used fine sand of 100 μm size at 1wt.% concentration. Using a combination of hard band-pass filtering for the analog signal and a wavelet threshold de-noising algorithm for the digital signal, they were able to filter out the noise from other sources in the signal and improve signal to noise ratio for sand signals about 30%.

This work develops from the results described by Droubi and Reuben [11] in which a relatively traceable way of measuring the total AE impact energy associated with particle-laden flow was proposed as a diagnostic impingement indicator for practical cases. However, this work uses a

new model based on the static and oscillatory parts of the AE signal for particle free water flow in a laboratory flow loop, using demodulated spectral analysis. Those parts of the signal are then removed from signals acquired for tests with water flowing at a range of flow rates and where a range of sand fractions and quantities are included. This enhances the temporal sensitivity of the AE technique and enables identification and quantification of sand in these laboratory tests.

2. Experimental method

Figure 1 illustrates schematically the experimental set-up, and this is described in detail by Droubi and Reuben [11]. The flow loop consisted of a positive displacement pump (model C22BC10RMB, Mono™ pump driven by a 1.1 kW geared motor to give an output speed of 587 rpm), standard 23 mm PVC piping, a 50 litre conical tank and choke valves. The pump was chosen due to its ability to handle fluids with high concentration of solids up to 10 wt%, also to eliminate any pulsatile flows. The slurry was first mixed by recirculating it through a by-pass leg for around 20 minutes to ensure that all the solids were suspended in the flow before diverting the flow to the bend.

A sharp 90 degree bend (measurement cell) made from 5 mm bore carbon steel was inserted into the 23 mm bore PVC pipeline system in order to localize the impingement area and minimize the impact angle range. The bend wall opposite to the stream was milled flat to assist sensor mounting and machined to give 7 mm wall thickness at the site where the sensor was mounted. A broad band piezoelectric AE sensor (Micro-80D, Physical Acoustics Corp.) was coupled by means of high vacuum grease onto the outside surface of the bend directly above the impingement area then clamped onto the bend using a magnetic clamp. The sensor was 10 mm in diameter, and produces a relatively flat frequency response across the range (0.1 to 1 MHz) and operates in a temperature range of -65 to 177^{o} C. The signal from the AE sensor was pre-amplified (PAC series 1220A with switchable 20/40/60 dB gain and integral band pass filter between 0.1-1 MHz) and AE records were acquired during impingement at a sampling frequency of 2.5 MHz for a duration of 1 second at full bandwidth. Prior to testing, the sensitivity of the sensor was checked by performing a pencil lead break test [13] at the bend to check the functioning of the AE detection system and to confirm the quality of sensor coupling. The AE energy measured was based on at least ten repeats for each particle size range tested. Following each set of experiments with a given particle loading, the rig was drained and cleaned.

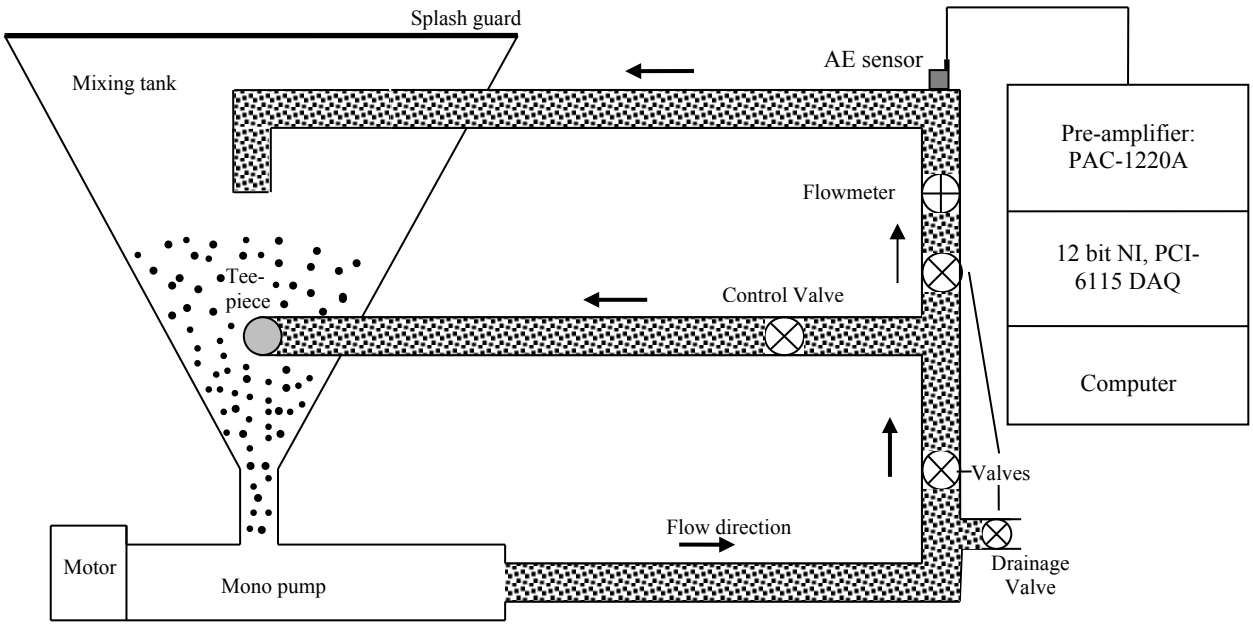

Figure 1: Experimental setup (slurry jet test apparatus) and measurement system.

Silica sand slurry was made from 10 litres of clean water and a predetermined mass of different particle size fractions in order to obtain the required concentration. In order to compare the results from this work with the previous works by the authors, the same test conditions as was used by [11] were chosen here. Four different particle size fractions were used (212-250 μm, 300-425 μm, 500-600 μm and 600-710 μm) and, for each fraction, an impingement run was carried out with a total of three levels of solid concentration, C, (1, 2.5, and 5wt.%), where wt.% is the percentage concentration of solids by weight in the slurry, and four different flow velocities, v, (4.2, 6.8, 10.2, and 12.7 ms^{-1}). The nominal concentration of the particles in the suspension was based on the amount added to the rig. For all test runs ten AE signals were acquired which resulted in analysis of over 1300 acquired AE signals.

3. Analysis

An essential aspect of AE monitoring is to be able to establish the physical phenomena which generate the AE. In the case of particle-laden flows, the phenomenon of interest is particle impact with the pipe walls, although there may well be other sources (such as that caused by turbulent flow and electrical interferences). Therfore, the first step in enhancing the practicality of a sand monitoring system and to avoid a false interpretation of recorded AE data is by identifying the type of propogation behaviour shown by the wave generated from particle-free water impingement, as well as understanding any time or frequency domain characteristics introduced by operational flow conditions in the acquired AE signals.

i. Analysis for particle-free water

Figure 2 shows samples of typical raw AE signals recorded for water impingement along with typical raw AE spectra over the range of flow speeds tested. It is clear that the raw AE signal amplitude, in general, increases with increasing flow speed. The effect of the sensor bandwidth is apparent in the raw frequency spectrum, with most energy being contained in the range 100-400 kHz. The spectra show that most of the power is focused in three bands; one very narrow band centred on a frequency of around 100 kHz and characterised by a spike at the lowest speed whose magnitude decreases rapidly with increasing flow speed, a band at 150 kHz to 200 kHz, and another band at 300 kHz to 400 kHz. There is also a small component at 600 kHz at 12.7 ms^{-1} flow speed. It is also clear that, within its bandwidth, the sensor shows a systematic shift in frequency content (power) towards the higher end as the flow speed increases. To quantify these systematic changes in raw AE frequency content, the proportion of the total energy in these three frequency bands was determined, for each of the 20 AE records at each flow speed. **Figure 3** shows the variation in AE energy proportion in each band with flow speed where each point represents the average of 20 AE records along with the standard deviation. As can be seen, the first band decreases rapidly with flow speed while the highest frequency increases with speed. Thus, raw AE frequency analysis can potentially offer a means of monitoring flow speed.

	Raw AE signal	Frequency spectrum
(a)	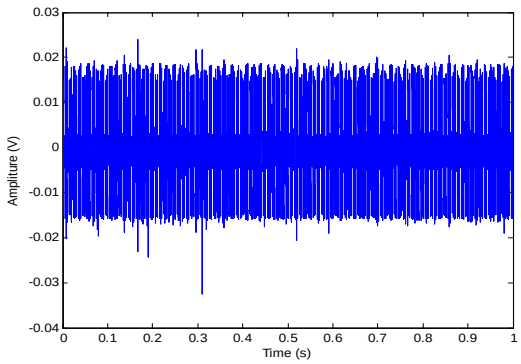	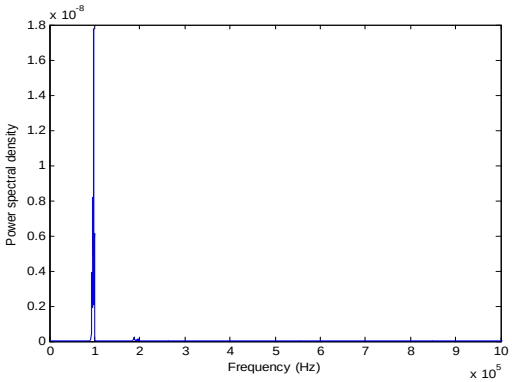
(b)	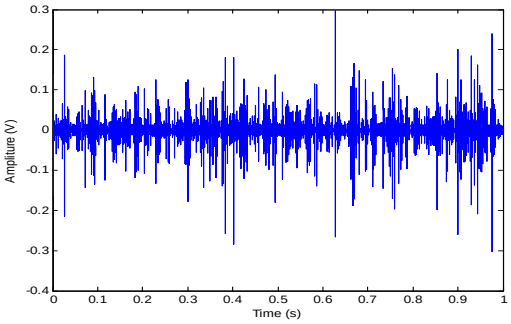	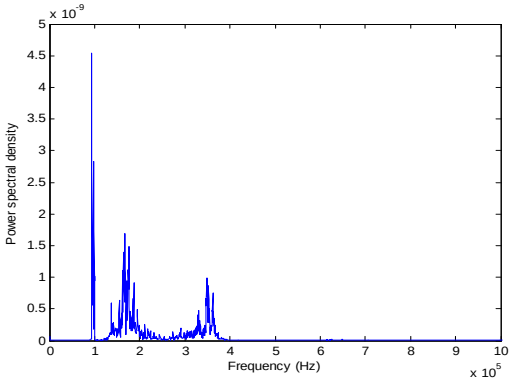
(c)	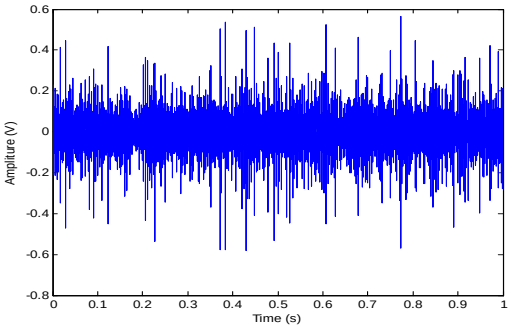	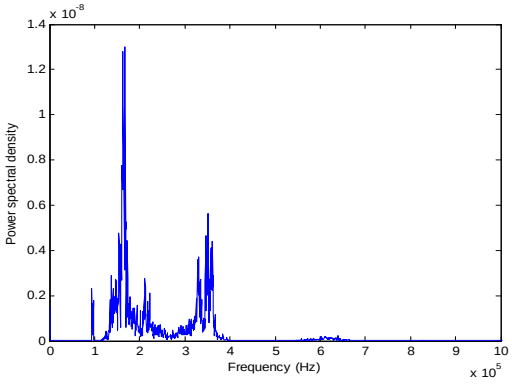

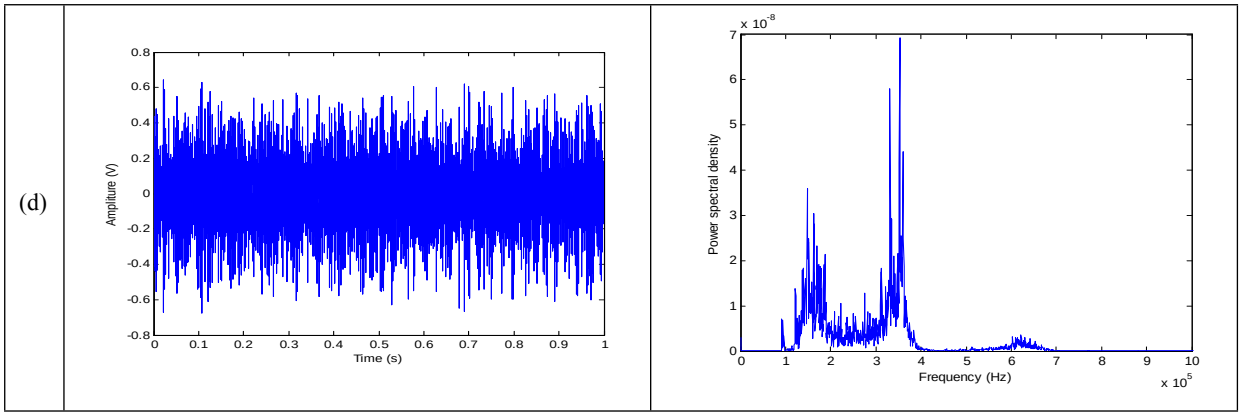

Figure 2: Typical 1-second raw AE time series for water impingement in the flow loop and their corresponding raw frequency spectra for flow speeds: (a) 4.2 ms^{-1}, (b) 6.8 ms^{-1}, (c) 10.2 ms^{-1}, and (d) 12.7 ms^{-1}

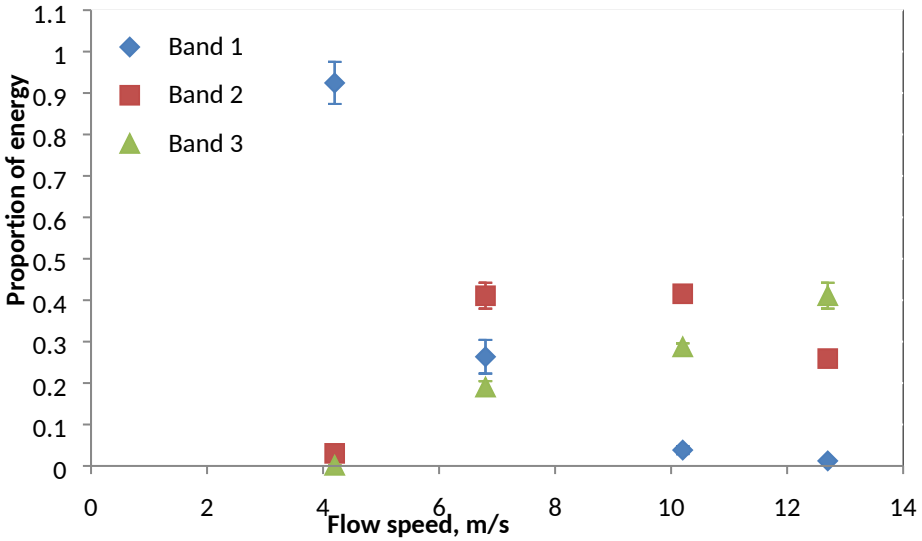

Figure 3: Proportion of AE energy in raw frequency bands versus flow speed; Band 1: 100 kHz, Band 2: 150-200 kHz, Band 3: 300-400 kHz

Figure 4 shows a magnified 0.1-second segment of the record depicted in **Figure 2a** in both raw and averaged forms. It is clear that the hydraulic conditions produce a strong pulsatile nature to the particle-free time series which can be seen as a carrier wave for the particle signatures. Dealing with such pulsatile signals requires a demodulated analysis of the signals to make use of the periodicity. Also, these signals suggest a strong influence of fluid pulses on the recorded AE with a pulse period of around 100 Hz, associated with the rotational speed of the pump, 10 Hz, and the helical geometry of the pump impeller.

(i) (ii)

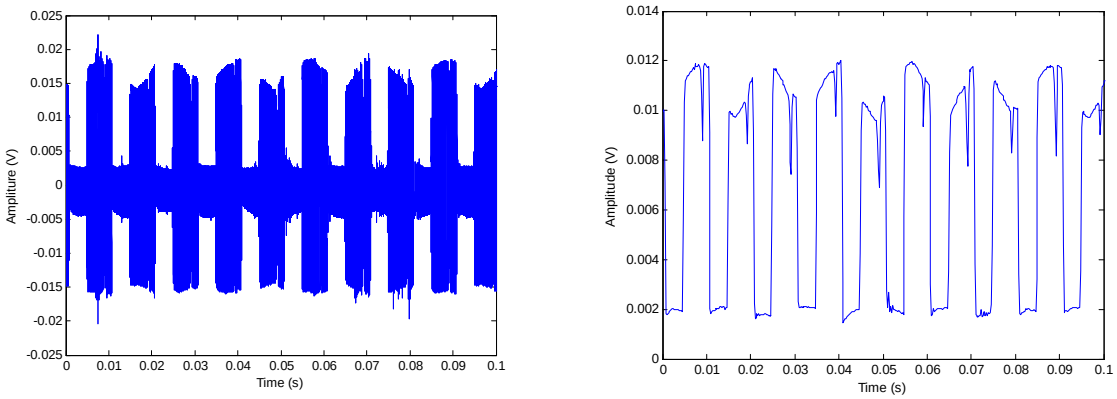

Figure 4: Magnified view of 0.1-second segment of the signal shown in **Figure 2a** (i) raw AE signal and (ii) RMS AE signal

To investigate the lower frequency characteristics of the water impingement signals, demodulated frequency analysis was developed in MatLab and applied to all signals at all flow speeds tested. First, the raw AE signals were averaged with a 0.2 ms averaging time (over 500 points) using a root mean square (RMS) algorithm, making the effective sampling rate 5000 samples per second as shown in **Figure 4ii**. Then, the RMS AE signal was made bipolar by subtracting the mean value of the record from each point in order to remove the DC component before transforming the signal into the frequency domain. Finally, all spectra were normalized to unit energy content in order to facilitate comparison.

Figure 5 shows typical examples of the resulting normalized RMS AE signals along with the corresponding normalized frequency for water impingement for each of the flow speeds tested. The frequency domain at the lowest flow speed, **Figure 5a**, shows spectral peaks occurring at relatively regular frequency intervals which imply the possibility of one fundamental frequency component with other peaks resulting from harmonics. On closer inspection, it was found that two spectral peaks are dominant; 100 Hz at the lowest flow speed and 42 Hz at the highest flow speed, **Figure 5d**. Between the two extreme speeds, the energy in the 100 Hz peak decreases with speed while the 42 Hz increases. The spectra at the intermediate speeds show a transition between the two extremes, **Figure 5b** showing both spectral peaks and **Figure 5c** exhibiting a broad demodulated frequency spectrum.

At first sight, the complexity of what is essentially a noise pattern might make the identification of particle impact signatures a daunting prospect. However, a clear understanding of this

pattern assists in separating signal from noise, but also allows the exploration of the potential to use the low frequency as a carrier wave.

	RMS AE signal	Normalized Frequency spectrum
(a)	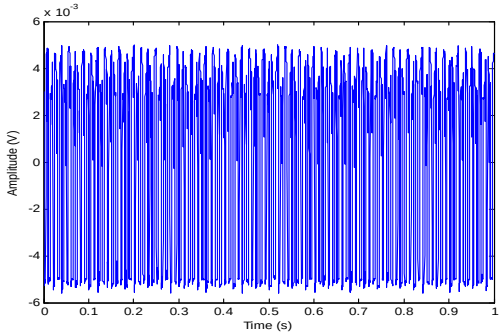	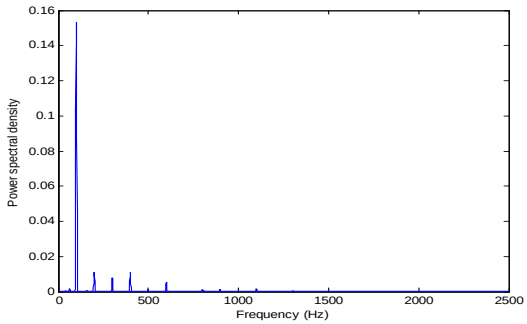
(b)	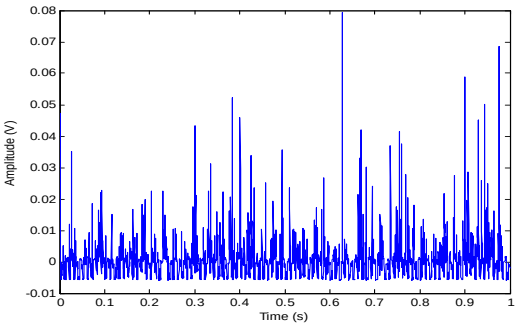	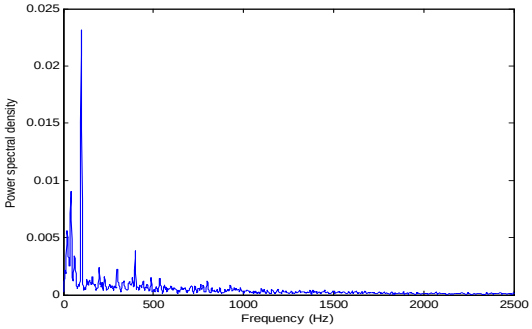
(c)	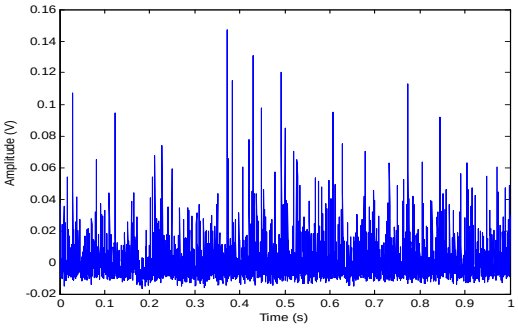	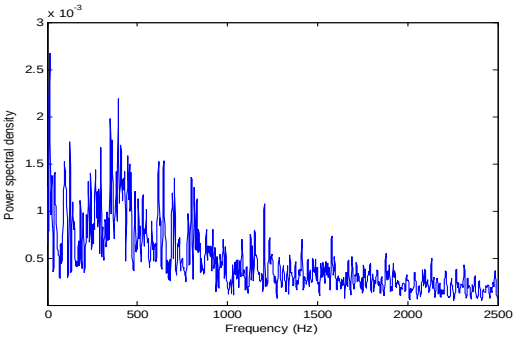

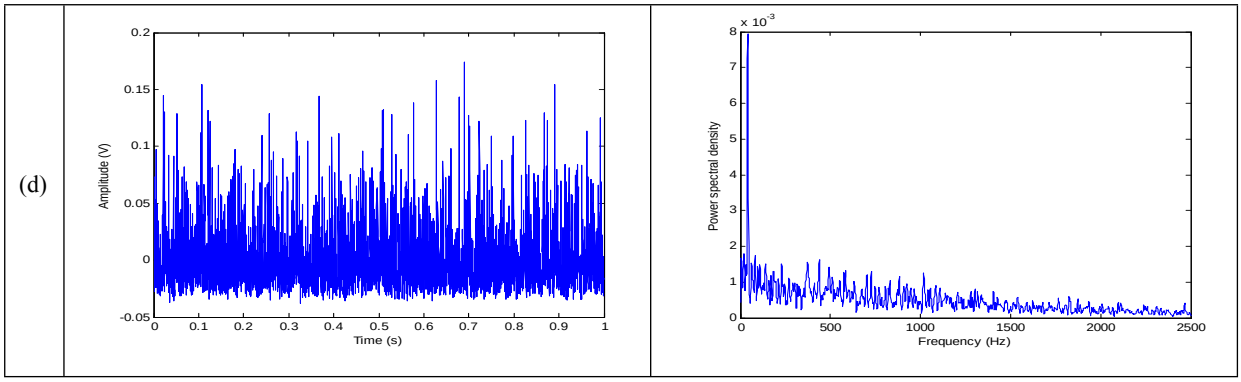

Figure 5: Typical 1-second RMS AE signals for water impact and their corresponding normalized demodulated spectrum for flow speeds: (a) 4.2 ms^{-1}, (b) 6.8 ms^{-1}, (c) 10.2 ms^{-1}, and (d) 12.7 ms^{-1}

In order to quantify these demodulated spectra, a processing approach was devised based on categorisation of peak heights and their corresponding frequencies. For each flow rate, across the 20 records, all peaks in the spectrum were identified automatically by first applying an identification threshold of 5% of the maximum peak heights and then obtaining each peak height and its corresponding frequency. The ten highest peaks in the spectrum were then taken along with their corresponding frequency values for each record. Next, the resulting 200 values of peak height and corresponding frequency for each combination were used as an input to a MatLab algorithm. The algorithm divided the frequency range into 20 Hz bins and allocated each peak height to the appropriate frequency bin, calculating the number of occurrences in each bin. The average peak height for each bin was then determined by dividing the sum of all peak heights by the number of occurences: $Average\ peak\ height = \frac{\sum peak\ heights}{number\ of\ occurences}$.

Figure 6 summarises the results, quantifying the two distinct frequency patterns described above. As can be seen in **Figure 6a** a very clear harmonic pattern occurs at low speed with a fundemantal frequency of 100 Hz and charactersied by a set of much smaller harmonics. At the next highest speed, **Figure 6b** a broader spectrum based on 42 Hz begins to emerge alongside the 100 Hz pattern noted in **Figure 6a**. At the highest speed, the 100 Hz pattern is absent and is replaced by the 42 Hz band plus some higher frequency components not on the 100 Hz series. The spectrum for the higher intermediate speed is slightly anomalous in that, although it contains a growing 42 Hz component, there are a number of other components present at higher intensity. Although the exact causes of these low frequency spectral behaviours are not entirely clear, it is likely that they are associated with the hydraulic and

resonant behaviour of the flow loop. The rotational speed of the pump is 10 Hz and the resonance frequency of the pipe was calculated [14] to be in the range 12 to 24 Hz depending on the boundary conditions, so this does not explain either the 42 Hz or 100 Hz frequencies, nor, indeed the very obvious pulsation at lower speed. In fact, the spiral shape of the mono pump impeller is specifically designed to eliminate flow pulsations. However, it is possible that any practical application will be on a system with its own hydraulic characteristics and geometry, so the flow loop provides an example of how such characteristics might be dealt with in attempting to monitor particle impingement.

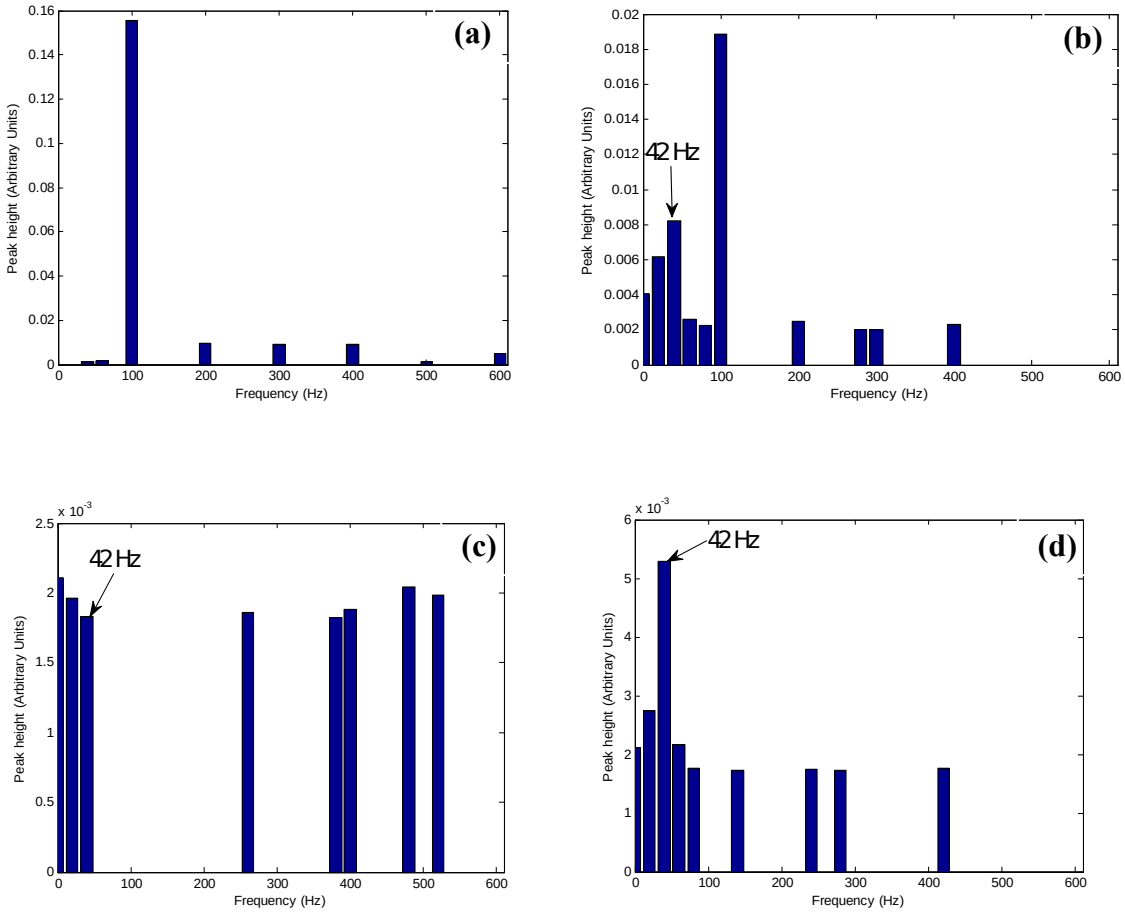

Figure 6: Distribution of the ten top frequency peak heights for water impingement at four flow speeds: (a) 4.2 ms^{-1}, (b) 6.8 ms^{-1}, (c) 10.2 ms^{-1}, and (d) 12.7 ms^{-1}

As is obvious from the foregoing, any model for the AE arising from water impingement will consist of an oscillatory component and a static component. Therefore the total AE energy was

divided into two parts, a static component E_{st} and an oscillatory component E_{osc}. The static component was simply obtained by calculating the average of the square RMS value of the entire AE record (1-second). The oscillatory part was obtained by integrating the RMS of the 1-second averaged records using $\int_0^t V^2_{RMS}(t)dt$,($V^2.sec$), once the static component had been removed (records such as those shown in **Figure 5**).

The proportion of oscillatory energy that is contained in the top 10 peaks for all flow speeds is shown in **Figure 7.** As can be seen, the remaining energy is quite high for the higher speeds, particularly in **Figure 7 (c)** where a lot of other energy in different frequency bands are apparent and in many cases of the same order of magnitude, indicating a generally more broadband distribution of energy.

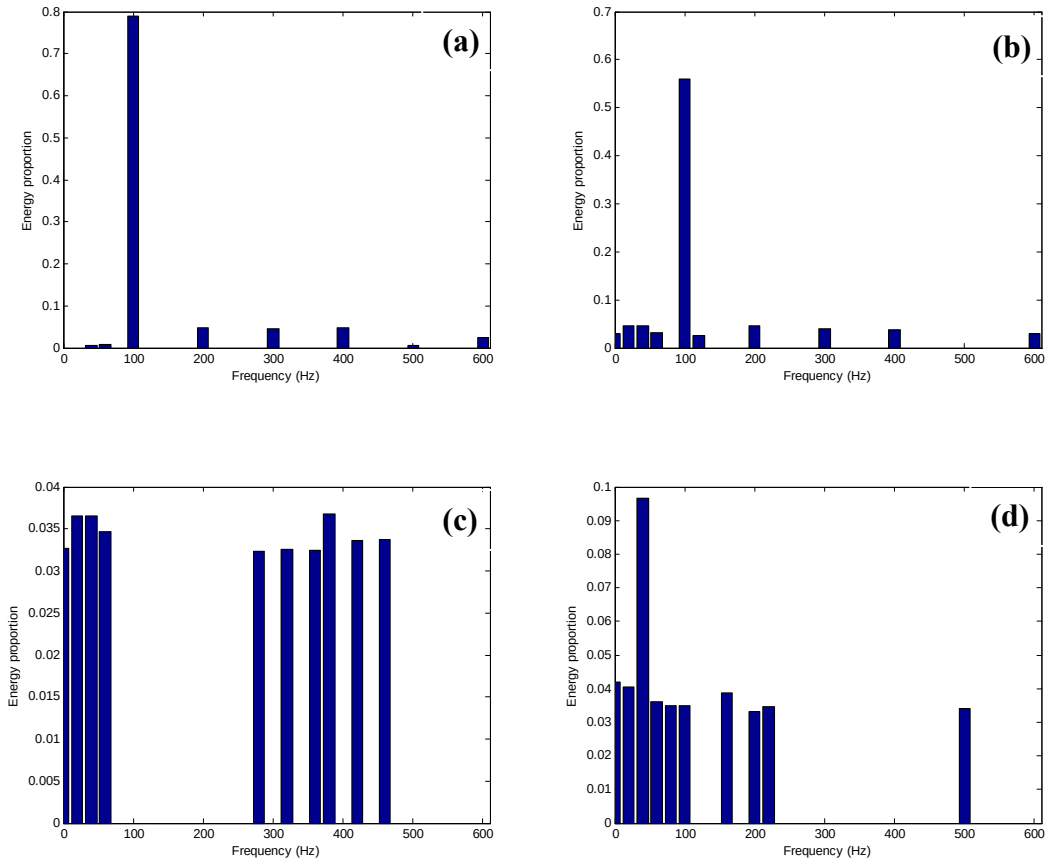

Figure 7: Proportion of the oscillatory energy contained in the top 10 peaks for water impingement at four flow speeds: (a) 4.2 ms^{-1}, (b) 6.8 ms^{-1}, (c) 10.2 ms^{-1}, (d) 12.7 ms^{-1}

Figures 8 and **9** show the effect of flow speed, v, on both the static and oscillated AE energy components, respectively, where each point represents the average of the 10 AE records and error bars represent the variation of the 10 records as standard deviation. Previous work [11] found a power law dependence between total AE energy and flow speed. However in this case an exponential relationship shows the best comparison between the static and oscillatory components of the AE energy and flow speed as shown in **Figures 8** and **9** where the horizontal axis is given as flow speed (v-4.1 m/s) which was used in the interest of obtaining a better fit. The best fit power equation is also shown for each AE component. Thus, the AE energy associated with water impingement can be described by a mean level $E_{st}^{w} = 0.0013exp[0.29(v-4.1)]$ and an oscillatory component of energy $E_{osc}^{w} = 0.0026exp[0.19(v-4.1)]$.

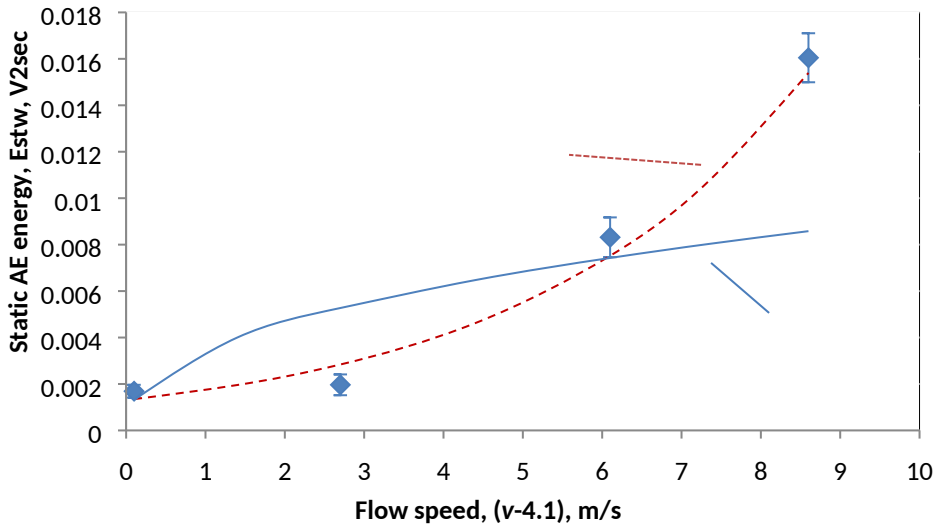

Figure 8: Effect of flow speed on static AE energy for water impingement showing the best power fit (solid line) and the best exponential fit (dashed line)

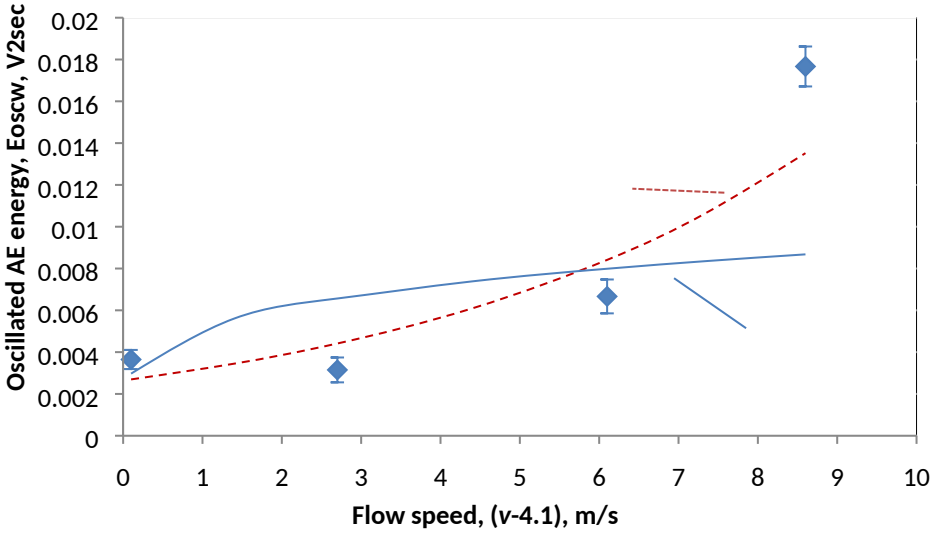

Figure 9: Effect of flow speed on oscillatory AE energy for water impingement showing the best power fit (in red colour) and the best exponential fit (in blue colour)

ii. Slurry impact analysis

A decomposition into static and oscillatory components was also used to analyse the AE acquired from particle-laden flow tests as shown in Figure 10. The total AE energy for each record, $\boldsymbol{E_{tot}^{sl}}$ was divided into its two main components the static component, $\boldsymbol{E_{st}^{sl}}$ and the oscillatory component, $\boldsymbol{E_{osc}^{sl}}$ in the same way as was done for particle-free water. Each of these can be further divided accordingly into components due to particles E^p and due to water and other mechanical sources E^w.

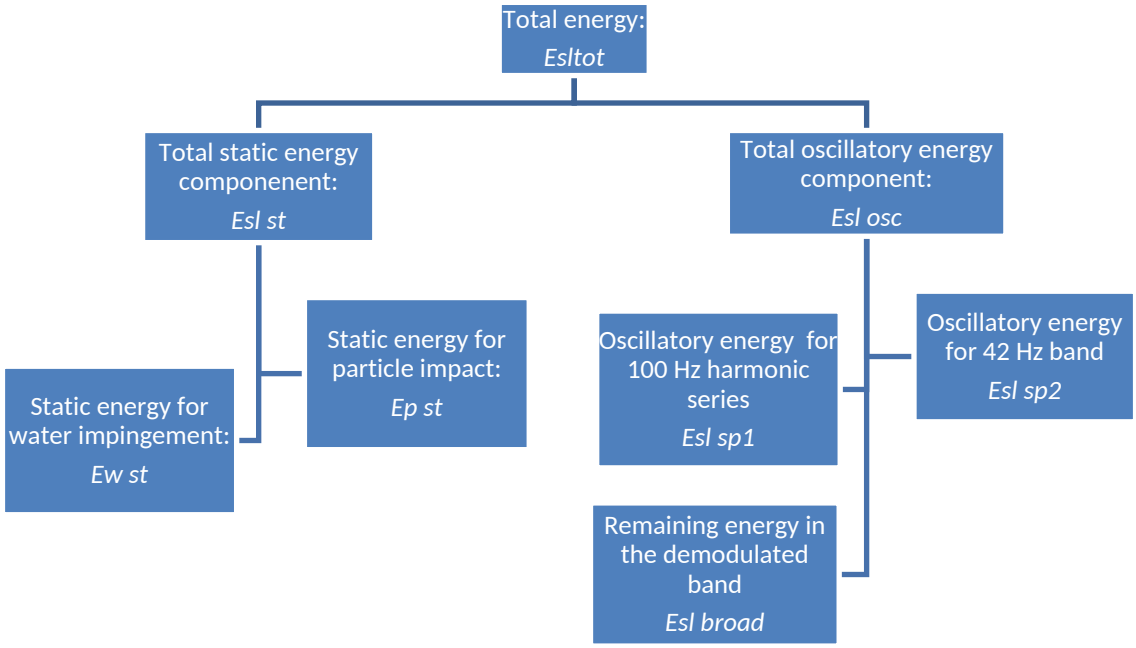

Figure 10: Schematic illustration of the decomposition of slurry impingement AE energy in the flow loop

The static AE energy associated with particle impact, E_{st}^{p}, can be determined by subtracting the actual average values of the static energy of water impingement **Figure 8**, E_{st}^{w}, from the total static energy of the slurry E_{st}^{sl} as: $E_{st}^{p} = E_{st}^{sl} - E_{st}^{w}$.

In order to examine if the energy for slurry impingement is carried in the same frequency bands as water impact, the dynamic slurry energy, E_{osc}^{sl} was divided into three parts, the component associated with the 100 Hz harmonic series, E_{sp1}^{sl}, the component associated with the 42 Hz band, E_{sp2}^{sl}, and the remainder of the demodulated band, broad oscillatory component, E_{broad}^{sl} (see **Figure 10**),

$$E_{osc}^{sl} = E_{sp1}^{sl} + E_{sp2}^{sl} + E_{broad}^{sl} \qquad (1)$$

To decompose the oscillatory part of the AE, each record was band-pass filtered twice in the sp_1 and sp_2 bands using an infinite impulse response (IIR) digital filter of Chebyshev Type I , set with a fifth order low pass digital Chebychev filter and 0.9 peak to peak ripple in the passband [15].

There is a general agreement [8] that AE energy is proportional to the incident particle impact energy (½ mv^2) that dissipates as elastic waves through the target material, so the normal expectation that AE energy associated with particle impacts will depend on the square of the impact speed. **Figure 11** shows an example of the effect of flow speed on the static AE energy associated with particle impacts E_{st}^{p} for maximum particle size fraction and all nominal concentrations tested. At least ten repeat 1 s records were analysed for each experimental condition where each point represents the average value of the ten recorded AE energy along with its standard deviation. As explained in section 2 the results are based on the analysis of over 1300 acquired AE signals. As can be seen, the static AE energy increases with both flow speed and nominal concentration with approximately the second power of the flow speed, although the best power fit is not satisfactory at the lowest concentration tested.

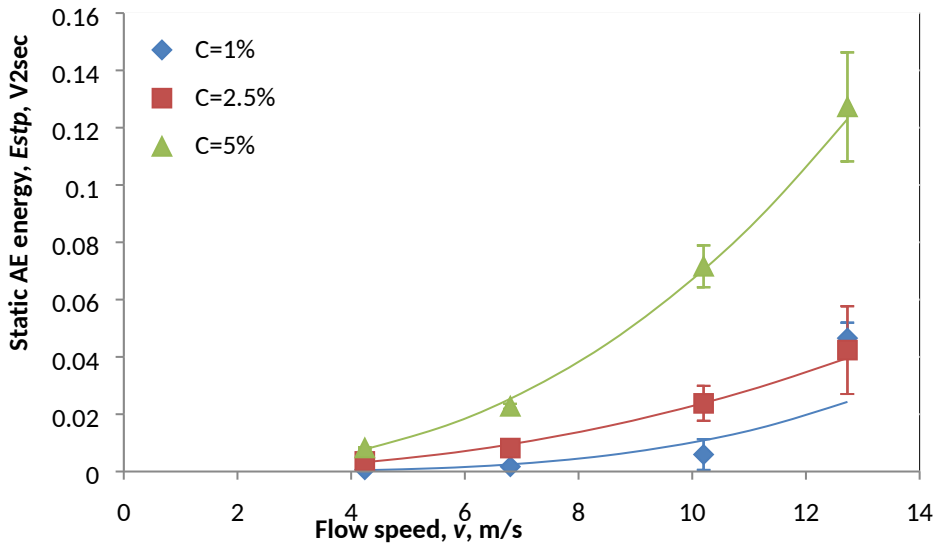

Figure 11: Effect of flow speed on the static AE energy for the three concentrations for particle size fraction 600-710 µm

The variation of the best fit power index n, calculated using $y = Ax^n + B$, for all experiments along with the respective curve fitting (R^2_i) that were determined by curve fitting are also summarised in **Table 1** which shows the weighted average exponent that calculated from $\bar{n} = \frac{\sum n_i R_i^2}{\sum R_i^2}$ to be 2, which is in reasonable agreement with other studies which report this index to vary in the range of 1.5-3 depending on the slurry properties and mechanical properties of the material under investigation [16]. The variation in the flow speed power index might be

explained by the fact that the slurry in the flow loop was directed vertically against the elbow, so flow streams that are directed in an upward direction will have the vertical component of their velocity affected more than the horizontal, leading to lower impingement angle and lower than expected *n* values, and this would be expected to affect smaller particles more than large ones. As can be seen from **Table 1**, generally, the flow speed exponent tends towards the expected value of 2 for all particle size ranges except for the lowest size fraction where exponent tends towards 1 (where the signal to noise ratio might be expected to be the lowest). Nevertheless, the lower than expected exponent observed here was not possible in [11] where no trend between recorded AE energy and flow speed was determined, proving the feasibility of using the proposed decomposition technique in sand impact detection.

Table 1: Power index of flow speed dependence of the static component of measured AE energy for all flow loop tests (bold text data are shown in **Figure 11**)

Particle size range (μm)	Nominal concentration (kg/m^3)	Flow speed power index (n)	Curve fitting R^2 value (%)
212-250	1	1.18	75
	2.5	1.22	82
	5	1.03	93
300-425	1	2.6	93
	2.5	1.8	97
	5	1.95	93
500-600	1	2.1	78
	2.5	2.2	86
	5	2.3	87
600-710	**1**	**3.6**	**89**
	2.5	**2.2**	**99**
	5	**2.5**	**99**

Figures 12 to **14** show the variation of the energy in each spectral component (i.e. the 100 Hz band E_{sp1}^{sl} , the 42 Hz spectral component E_{sp2}^{sl} and the broad oscillatory component E_{broad}^{sl}) with flow speed for all particle size fractions and solid concentrations tested, along with the corresponding components for particle-free water. Again each point the average value of the ten recorded AE energy along with its standard deviation. The 100 Hz band E_{sp1}^{sl} which is

attributed to mechanical noise is shown in **Figure 12** and the results are not sensitive to the presence of sand particles except at the lowest flow rate (circled in red) where the particle impact signal/noise ratio might be expected to be largest. The 42 Hz spectral component E_{sp2}^{sl} which is due to fluid flow is shown in Figure 13. As can be seen, this component is always very small and increases with flow speed. There is very little difference between the the results for the various particle size fractions and concentrations and water only results for this component, so it is of little use in detecting particle impacts.

The dominant band is the broad oscillatory component E_{broad}^{sl} , as can be seen in **Figure 1**4, which is a magnitude of order higher than the other two components**.** The results are generally more consistent with the component E_{broad}^{sl}, increasing with flow rate, less sensitive to particle fraction size and varying trends with concentration.

Unlike all the other spectral components, the 100 Hz band decreases with flow speed. **Figure 15** shows the effect of particle size and concentration on this spectral component at the lowest flow speed. As can be seen, the 100 Hz spectral component decreases with both the nominal particle concentration and particle size range indicating that the pump rotational speed effect on the AE recorded can be obscured by more particles in the mixture or bigger particle size range. It is also evident from **Figure 14,** which shows the best fit power index *n* for all of the measurements, that velocity exponents in the range 1.6 to 3.1 are associated with the broad oscillatory component and particle signal (above the water "noise") is much clearer at higher concentration and particle size ranges.

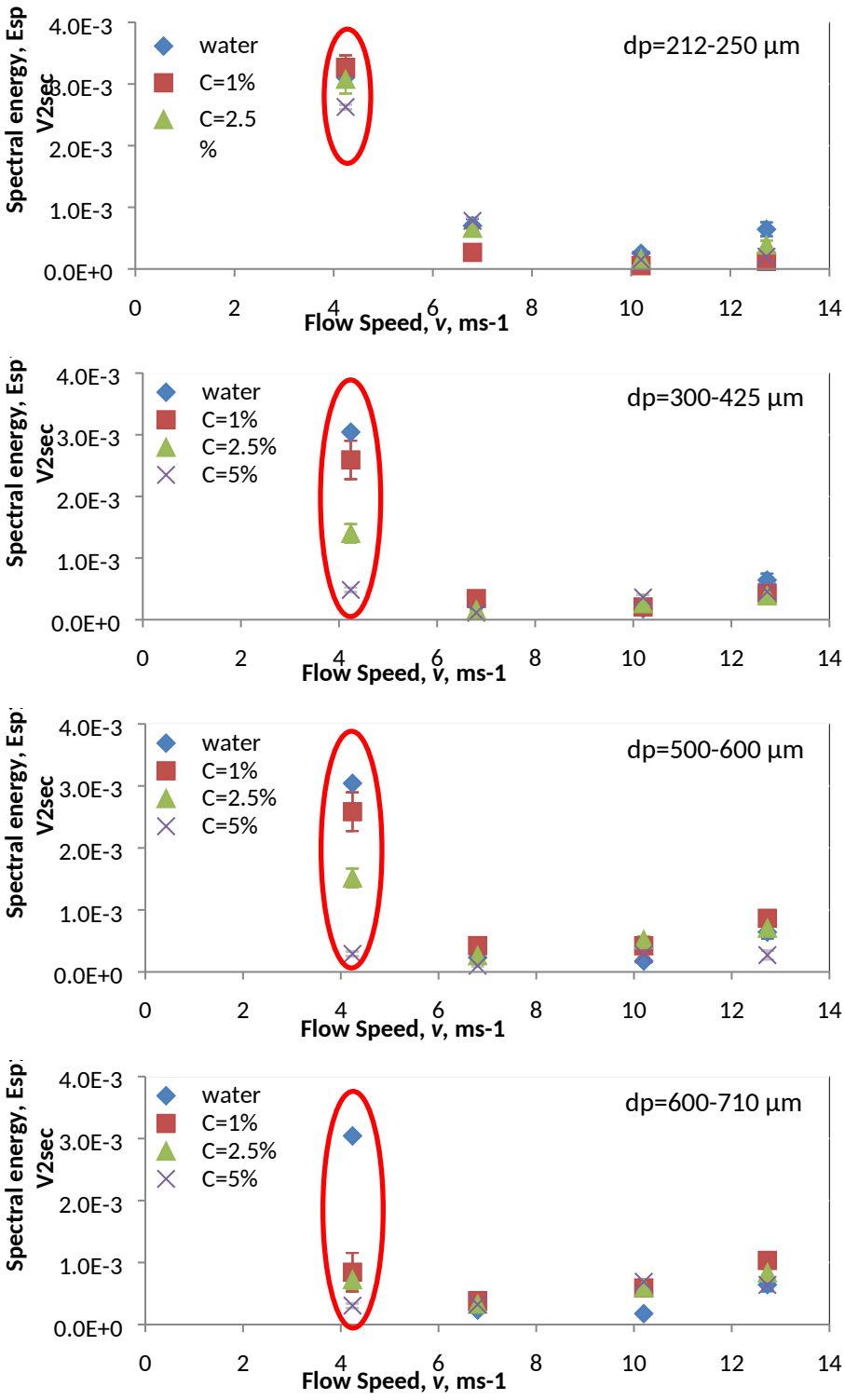

Figure 12: Effect of flow speed on the spectral AE energy, E_{sp1}^{sl}, for the three concentrations and particle-free water for each of the particle size fractions shown

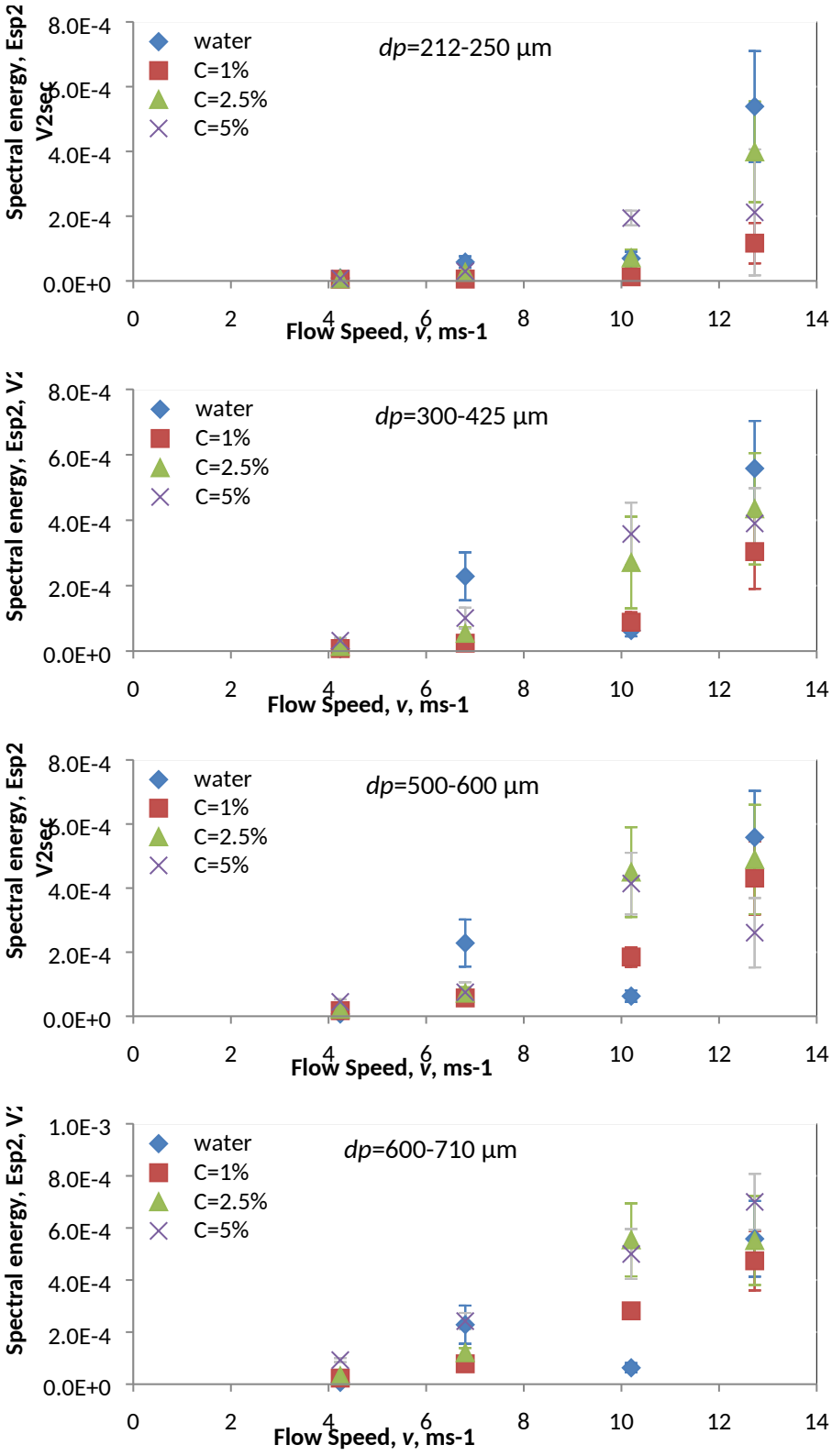

Figure 13: Effect of flow speed on the spectral AE energy, E_{sp2}^{sl}, for the three concentrations and particle-free water for each of the particle size fractions shown

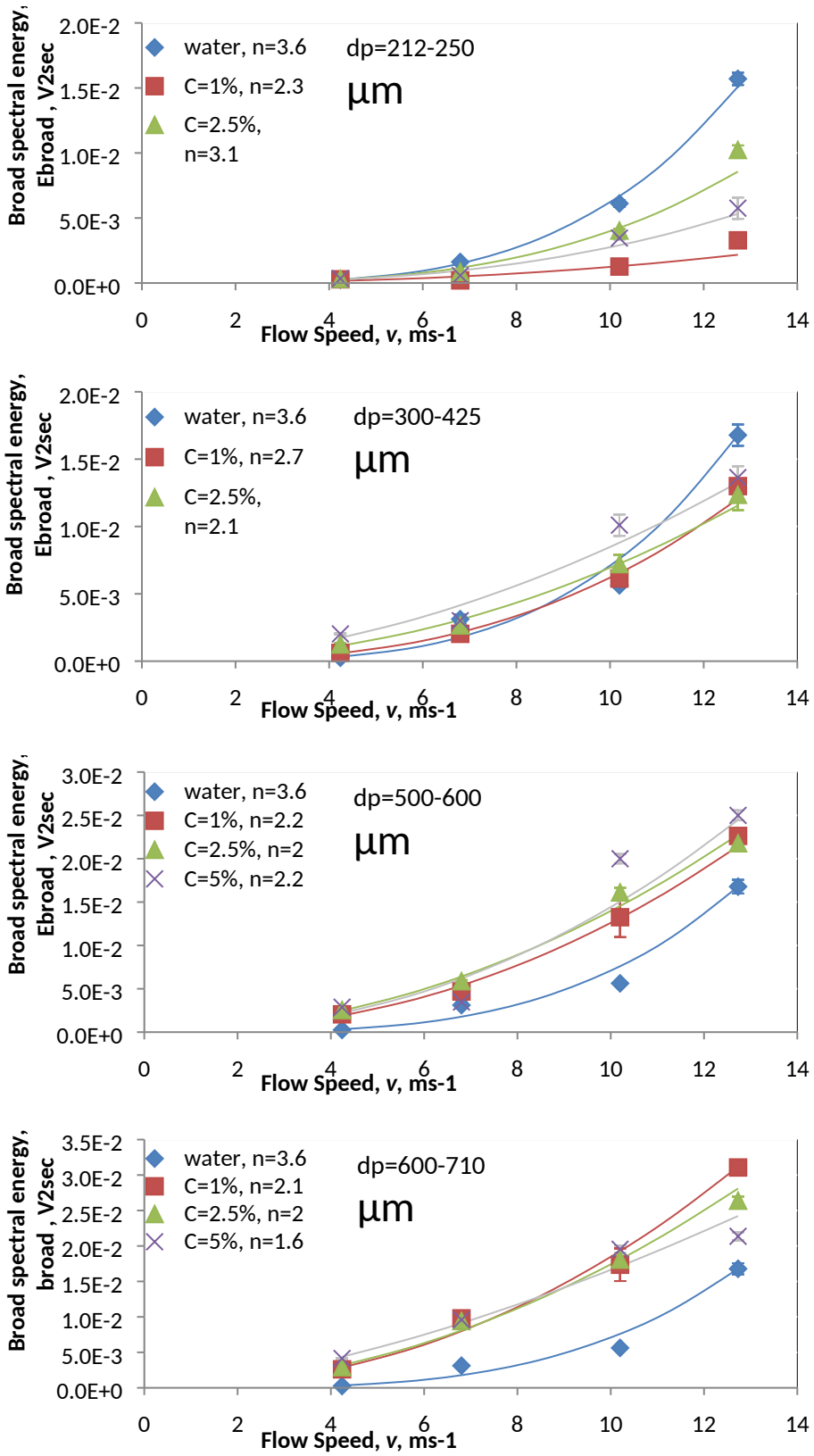

Figure 14: Effect of flow speed on the broad spectral AE energy, $\boldsymbol{E}_{\boldsymbol{broad}}^{\boldsymbol{sl}}$, for the three concentrations and particle-free water for each of the particle size fractions shown

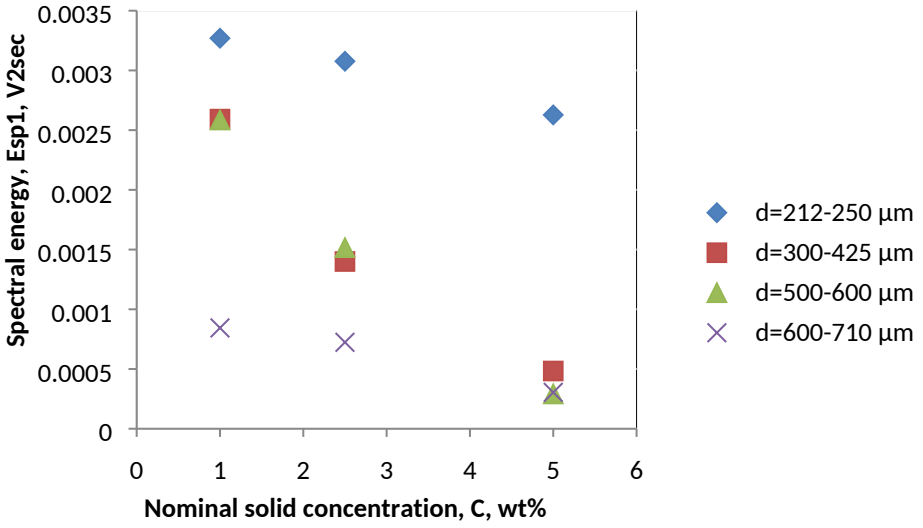

Figure 15: Effect of particle size and concentration on the spectral AE energy, E_{sp1}^{sl}, for each of the particle size fractions at 4.2 ms^{-1} flow speed

The general approach of developing a simple model for water impingement AE energy relative to flow speed and based on the static and oscillatory parts of the signal provides a means of characterising noise/interference sources in pipeline flows which has significant industrial and research applications. Although the results presented here are limited to the current piping system, flow rates, concentration, particle size and fluid properties tested, the overall approach of identifying static and spectral components of flow noise and structural vibration can be applied in any industrial application. Thus, a given application on an industrial installation would require any individual monitoring cell(s) to be designed to account for simultaneous flow noise identification leading to enhancement in the level of confidence for AE data interpretation. Such flow noise either hydraulic or mechanical are part of the acquired AE signal and the signal noise discrimination principle demonstrated in this work could be used to filter out unwanted noise/interference sources for continuous AE monitoring during petrochemical production where the presence of high operation noise is highly likely.

Conclusion

Acoustic emission has been used to characterize flow noise in a pipe where sand particles are impinging on a carbon steel bend, with the aim of enhancing monitoring of sand particle

impacts in a multi-phase flow-loop. Previous work identified AE associated with sand particle impingement in fluid flow in a pipe in the presence of other AE sources such as fluid flow and other mechanical vibrations. This work however presents a method of removing other noise components associated with fluid flow and mechanical vibration and, hence, enhances the ability to monitor sand particle impact with the following broad findings:

1. AE recorded by a sensor mounted on a pipe bend was strongly influenced by flow noise attributed to the hydraulic conditions in the pipe.

2. The raw AE power spectral density at 100 Hz varied systematically with the flow speed which indicates the potential of using AE as a measure of flow speed.

3. Demodulated frequency analysis of the water only impingement signals at different speeds showed two distinct components with spectral peaks at 100Hz and 42 Hz in the demodulated signal associated with mechanical vibration and fluid flow, respectively.

4. AE energy decomposition coupled with spectral peak filtering has been used to remove the static, E_{st}^{p} , and oscillatory, E_{broad}^{sl}, noise components in the signals, and hence improve the temporal sensitivity of acquired AE signals and subsequently improve signal to noise ratio in AE based monitoring systems.

5. Both these components increased proportional to v^n where n is typically between 1.5 and 3. In previous work [11] noise prevented this analysis at low flow speed and low particle size fractions, however this work has confirmed this relationship for these lower flow speeds and particle size fractions. This also now agrees with the results of previous work using slurry impingements and airborne sand particles [8, 10].

References

1. J.W.Martin, BP-Amoco erosional guidelines revision 2.1, 1999
2. R.J.K.Wood, T.F. Jones, Investigations of sand-water induced erosive wear of AISI 304L stainless steel pipes by pilot-scale and laboratory-scale testing, Wear 255 (2003) 206–218.

3. Folkestad T and Mylvaganam K S. *Acoustic measurements detect sand in North Sea flow lines.* Oil and Gas Journal, 1990.
4. Gao G, Dang R, Nouri A. Jia H, Li L, Feng X, Dang B, *Sand rate model and data processing method for non-intrusive ultrasonic sand monitoring in flow pipeline.* Journal of Petrolum Science and Engineering, 134 (2015), pp. 30-39
5. Wang K, Liu Z, Liu G, Yi L, Liu P, Chen M and Peng S, *Vibration sensor approaches for sand detection in oil–water–sand multiphase flow.* Powder Technology, 276 (2015), pp.183-192
6. Wang K, Liu Z, Liu G, Yi L, Yang K, Liu R, Chen M and Peng S, *Vibration sensor approaches for the sand detection in gas–sand two phases flow.* Powder Technology, 288 (2016), pp.221-227
7. Wang K, Liu Z, Liu G, Yi L, Yang K, Peng S and Chen M, *Vibration Sensor Approaches for the Monitoring of Sand Production in Bohai Bay*. Shock and Vibration, vol. 2015, Article ID 591780, 6 pages, 2015. doi:10.1155/2015/591780
8. Droubi M G, Reuben R L and White G, *Acoustic Emission (AE) monitoring of abrasive particle impacts on carbon steel.* Proceedings IMechE, Part E, Journal of Process Mechanical Engineering, 2012, **226**(3), pp. 187-204.
9. Droubi M G, Reuben R L and G. White, *Statistical distribution models for monitoring acoustic emission (AE) energy of abrasive particle impacts on carbon steel.* Mechanical Systems and Signal Processing, 2012, **30**, pp. 356-372.
10. Droubi M G, Reuben R L and G. White, *Monitoring acoustic emission (AE) energy in slurry impingement using a new model for particle impact*. Mechanical Systems and Signal Processing, **62-63,** (2015), pp. 415-430.
11. Droubi M G and Reuben R L, *Monitoring acoustic emission (AE) energy of abrasive particle impacts in a slurry flow loop using a statistical distribution model*. Applied Acoustics, 113, (2016), pp. 202-209
12. Husin S, Addali A, and Mba D, Feasibility study on the use of the Acoustic Emission technology for monitoring flow patterns in two phase flow. Flow Measurement and Instrumentation, 33, (2013), pp. 251-256
13. Hsu NN and Breckenbridge FR. Characterisation and Calibration of Acoustic Emission Sensors. Materials Evaluation. 1981; 39: 60 - 8.
14. Thomson, W Tyrrell; Theory of vibration with applications, 4th edition, CHAPMAN&HALL

15. N. H. Faisal, R. Ahmed, R. L. Reuben, B. Allcock, AE monitoring and analysis of HVOF thermal spraying process, Journal of Thermal Spray Technology, 20(5), 2011, p. 1071-1084
16. Ferrer F, Idrissi H, Mazille H, Fleischmann P and Labeeuw P. *On the potential of acoustic emission for the characterization and understanding of mechanical damaging during abrasion-corrosion processes.* Wear, 1999. **231**(1): p. 108-115.